

μ SmartScope: 3D-printed Smartphone Microscope with Motorized Automated Stage

Luís Rosado¹, João Oliveira¹, Maria João M. Vasconcelos¹, José M. Correia da Costa², Dirk Elias¹ and Jaime S. Cardoso³

¹*Fraunhofer Portugal AICOS, Rua Alfredo Allen 455/461, 4200-135 Porto, Portugal*

²*Instituto Nacional de Saúde Dr. Ricardo Jorge, Rua Alexandre Herculano 321, 4000-055 Porto, Portugal*

³*INESCTEC and University of Porto, Rua Dr. Roberto Frias, 4200-465 Porto, Portugal*

Keywords: Microscopy, Mobile Devices, Motorized Microscope Stage, Developing Countries, Mobile Health.

Abstract: Microscopic examination is currently the gold standard test for diagnosis of several neglected tropical diseases. However, reliable identification of parasitic infections requires in-depth train and access to proper equipment for subsequent microscopic analysis. These requirements are closely related with the increasing interest in the development of computer-aided diagnosis systems, and Mobile Health is starting to play an important role when it comes to health in Africa, allowing for distributed solutions that provide access to complex diagnosis even in rural areas. In this paper, we present a 3D-printed microscope that can easily be attached to a wide range of mobile devices models. To the best of our knowledge, this is the first proposed smartphone-based alternative to conventional microscopy that allows autonomous acquisition of a pre-defined number of images at 1000x magnification with suitable resolution, by using a motorized automated stage fully powered and controlled by a smartphone, without the need of manual focus of the smear slide. Reference smears slides with different parasites were used to test the device. The acquired images showed that was possible to visually detect those agents, which clearly illustrate the potential that this device can have, specially in developing countries with limited access to healthcare services.

1 INTRODUCTION

The increasing interest in the development of computer-aided diagnosis systems for disease diagnosis in developing countries is well known, mainly due to the common practical difficulties experienced in rural health facilities. The excessive workload due to shortage of medical staff has been reported as one of the most significant problems (Quinn et al., 2014), fact that has been driving the development of new solutions that aim to facilitate the diagnosis of several neglected tropical diseases.

The detection of several neglected tropical diseases, particularly blood stage parasites, are primarily based on well established and widely used laboratory techniques. The microscopic examination of smear preparations of different human biological products are also used to diagnosis a wide range of parasites, such as the usage of blood smears (e.g. Malaria, Lymphatic filariasis, African Trypanosomiasis), stool smears (e.g. intestinal helminths) and urine smears

(e.g. Schistosomiasis) (Utzing et al., 2012). However, reliable identification of the referred parasitic infections requires in-depth train for specimen preparation and high-standard expertise for subsequent microscopic analysis. Those requirements are closely related with the increasing interest in the development of computer-aided diagnosis systems for this purpose, particularly in the area of Mobile Health. The mobile phone is currently Africa's most important digital technology. In the year 2000 few Africans had a mobile phone, but today about three-quarters do (Zachary, 2015). So it becomes natural that Mobile Health is starting to play an important role when it comes to health in Africa, particularly through the usage of solutions that allow skipping over centralized laboratories (Dolgin, 2015) by taking advantage of the advanced imaging and processing capabilities of the new generation of mobile devices.

Thus, the development of new portable microscopic devices (and ideally low cost) is an area that can greatly improve the chances of the successful de-

ployment of computer-aided diagnosis solutions for disease diagnosis in the underserved areas (Rosado et al., 2016). Given also the increase possibilities coming from additive manufacturing, in this paper we report our efforts on the development of a 3D-printed microscope with a motorized stage, termed μ SmartScope, that can be easily coupled to a smartphone. The process will be to place the smartphone in the μ SmartScope along with the smear, and have the smartphone image sensor to acquire a set of magnified images autonomously. This collection of images could then be analyzed, either automatically through image processing approaches, or manually by a specialist on a remote location.

It worth mentioning that we took into account several particularities of the African reality during the design of this device, like the high customs taxes and import duties currently in practice in many African countries; this motivated us to favor solutions easy replicable in third world countries. Several others additional requirements were equally considered, like automating the device as much as possible, discarding the need of considerable expertise and train of the technician in terms of maneuvering the microscope, or supplying the energy needed for the illumination and/or any type of automation through the mobile device battery, thus discarding the need of an additional power source.

This paper is structured as follow: Section 1 corresponds to Introduction and presents the motivation and objectives of this work; Section 2 give a summary of the related work found on the literature; Section 3 describes each component of the device, namely the Optics, Illumination and Motorized Automated stage; Section 4 details the process of Autofocusing; In Section 5 the Results are presented; and finally the Conclusions are drawn in Section 6.

2 RELATED WORK

Some research has been made in the last years to develop cell-phone based systems that provide low-cost alternatives to conventional microscopy. The microscopy designs of the proposed systems can be separated in three different areas: lensless, on-lens and attachment-based approaches.

The lensless approaches are based on the principles of holographic microscopy, i.e. the microscopic images are reconstructed from the holograms captured by the cell-phone. This approach has the advantage of not requiring any lenses or optical component as well as obtaining images with large field-of-view (FOV). However, acceptable resolutions are only ob-

tained for small magnifications ($\sim 40x$ magnification, NA= 0.65 objective) and processing power is needed to reconstruct the image (Tseng et al., 2010; Pirnstill and Cot, 2015).

On-lens approaches usually employ a refractive element directly attached to the smartphone camera at the focus, or a ball lens mounted in front of the camera lens (Arpa et al., 2012; Cybulski et al., 2014). Despite being a low-cost alternative, the ball lens produces a spherical focal plane, which creates aberrations and reduces drastically the usable FOV. Moreover, magnification and radius of the ball lens are inversely linked, so in order to achieve 1000x magnification we need a ball lens with radius of 0.15mm (Cybulski et al., 2014), which can turn the mounting and alignment process with the camera lens really challenging.

The attachment-based approaches covers the majority of the solutions already reported on the literature, which requires coupling additional hardware to the cell-phone, such as commercial lenses or illumination modules (Smith et al., 2011; Switz et al., 2014; Pirnstill and Cot, 2015). This approach usually takes advantage of complex optical elements that allow achieving suitable resolutions at high magnifications (e.g. $\sim 1000x$), which increases the overall cost of the system, but is currently a requirement for the microscopic examination of several neglected diseases. With high magnifications also emerges the limitation of having a small FOV, thus requiring the development of mechanisms to move the smears in order to cover a large area of the specimen. Moreover, it was verified that the majority of reported works are designed for a unique cell-phone model, which can greatly compromise the adoption of the proposed solution.

In this work, we present a 3D-printed microscope that can easily be attached to a wide range of mobile devices models. To the best of our knowledge, this is the first proposed smartphone-based alternative to conventional microscopy that allows autonomous acquisition of a pre-defined number of images at 1000x magnification with suitable resolution, by using a motorized automated stage fully powered and controlled by a smartphone, without the need of manual focus of the smear.

3 μ SMARTSCOPE COMPONENTS

Since we wanted to achieve a cheap and easily replicable alternative to conventional microscopes that can be attached to smartphones, most of the device is 3D-printed (see Fig. 1). The proposed device can be divided in 3 major modules: the Optics; the Illumina-

tion; and the Automated Stage (see Fig. 2).



Figure 1: μ SmartScope with smartphone attached and malaria-infected blood smear inserted.

3.1 Optics

The selected commercial lenses used to construct the μ SmartScope were supplied by Bresser, a vendor that showed a good price-quality relation for the required optics. Particularly, we used the Planachromat 100x oil-immersion objective (Bresser #5941500) and the Wide Angle 10x Eyepiece (Bresser #5941700).

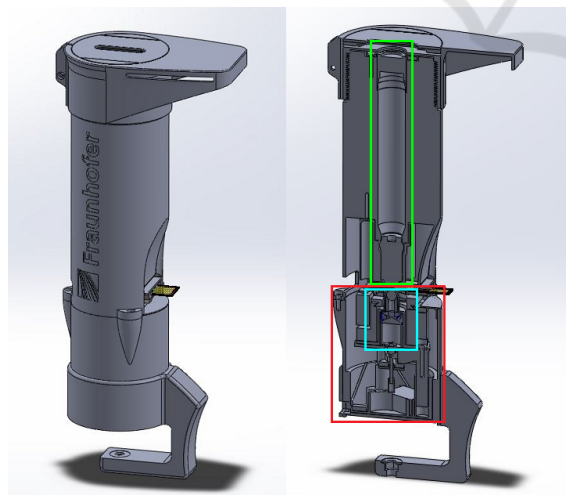


Figure 2: Render model of the μ SmartScope used for 3D-printing with the identification of the 3 main modules: Optics (green); Illumination (cyan); and Automated Stage (red).

3.2 Illumination

To allow a uniform illumination of the specimen, using just a LED is not enough because most of the light is lost to parts of the sample that are not being captured. To counter that, in a common microscope, a light condenser is normally used. The condenser is a lens (or multiple lenses) that concentrates the light from the illumination source and focus it in the part of the sample that is being captured by the amplification device. This device, in turn, magnifies the light beam, allowing an uniform illumination. Since the support materials for the lenses are 3D-printed, the minimum resolution of the 3D-printer must be taken into consideration. Several topologies of condensers can be used with their pros and cons. One of the cheapest options with acceptable results for our use case is the Abbe condenser, which uses a plano-convex lens to pre-concentrate the light into a smaller ball or half-ball lens that, in turn, provides the final concentration of light. This arrangement guarantees a good result by using cheaper individual lenses instead of an expensive, custom made, one. To design our condenser we selected a 20.4 x 25mm plano-convex lens (Edmund Optics #43483) and a 10mm N-BK7 Ball Lens (Edmund Optics #32748). In order to calculate the Back-Focal Length (BFL), i.e. distance on the optical axis between last active optical surface and the specimen plane (i.e. the sample), we used the following equation (Cybulski et al., 2014):

$$BFL = \frac{1}{2} \cdot \frac{r \cdot (2 - n)}{(n - 1)}, \quad (1)$$

where $r = 5mm$ is the radius of the ball lens and $n = 1.517$ is the Index of Refraction of the N-BK7 optical material. This gives a $BFL = 2.34mm$, as shown in Fig. 3.

Despite the distances defined on Fig. 3 being strictly respected, during the design we also had to ensure that the center of the ball lens was both carefully aligned with the center of the plano-convex lens and with the center of the objective lens.

3.3 μ Stage

The microscopic examination of smears usually requires the visual analysis of different microscopic fields (i.e. positions) of the smears, and the minimum number of required fields depends on the disease and used magnification. For instance, according to World Health Organization (WHO), the analysis of 100 fields of a blood sample is the minimum needed to perform a malaria microscopy test (WHO, 1991). Currently, this process is manually performed

by trained staff and can be extenuating, requiring that the operator takes regular breaks in order to ensure maximum attention. In order to improve this process, the sample movement should be performed autonomously and on-demand by the smartphone. For that, the μ Stage was developed, which is an automatic stage designed to be as cheap as possible, while providing displacement up to 20mm in X/Y with resolution of $500\ \mu\text{m}$ and a resolution of $25\ \mu\text{m}$ in the Z axis. It was designed to be powered using the USB-OTG connection of the smartphone.

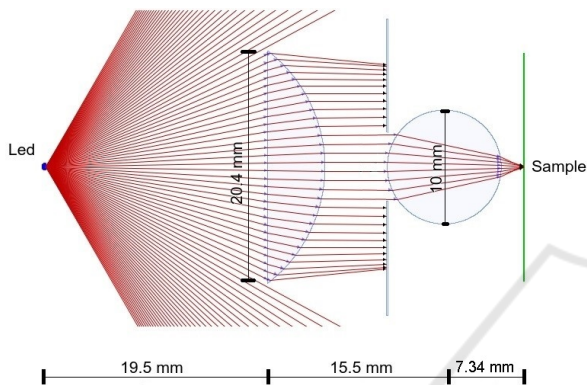


Figure 3: Schematic of the developed condenser generated with OpticalRayTracer® optics design software.

3.3.1 Mechanical Structure

In order to be as flexible as possible, most of the structure is modular and can be adapted without needing to refactor the whole structure. One of our major goals was to minimize the use of mechanical components and try to 3D-print as many parts as possible. This reduces costs and facilitates replication in third world countries, but has some disadvantages like reduced precision and wear.

The structure is composed by a base part where the electronic board, the Z axis actuator and the μ USB connector are placed. In this part, there are 3 slots that are the negatives of the tubular structures of Z axis. Besides the base, the stage is divided in 4 functional modules that are fully 3D printed (see Fig. 4):

- **Z axis:** Composed by 3 tubular structures that slide against their negatives in the base part, the Z axis was designed to have the highest resolution possible within the restrictions to ensure correct focus of the smear. Ensuring that the used 3D-printer is correctly calibrated and parametrized is evidently important for all μ SmartScope printed components, but particularly crucial for this module. Obtaining the required gap between the each

tubular structure and the corresponding negative is crucial to achieve a smooth Z axis movement, without tilting. Moreover, a simple stepper motor is used to provide the movement, being the circular movement translated through a M3 threaded rod and a nut fixed in this part. A rigid piece of heat shrink sleeve is then used to couple the stepper with the threaded rod. This ensures that eventual 3D printing deviations are corrected by the flexibility of the sleeve without compromising the Z axis movement.

- **X/Y axes:** Composed by 2 parts that slide against the Z axis module and between each other, the precision is not high but the resolution is enough to ensure at least 100 different microscopic fields. It should be noted that repositioning to a specific field location with high precision is usually not needed in microscopic smear analysis. Covering different microscopic fields that represents the overall specimen is by far much more important. Two servo motors are used to provide the movement, together with some rubber bands that ensure the movement in both ways. This arrangement is not linear since the servo movement is provided in a 90° arc, but ensures different fields: while one of the servo moves, the other is always static and placed in the Z axis part.
- **Illumination:** The optical design of this module was already presented in section 3.2, which passes through the Z and X/Y axes modules.
- **Smear holder** - a standard microscope slide can be fitted in the top part of the stage and hold in place by a simple plastic piece.

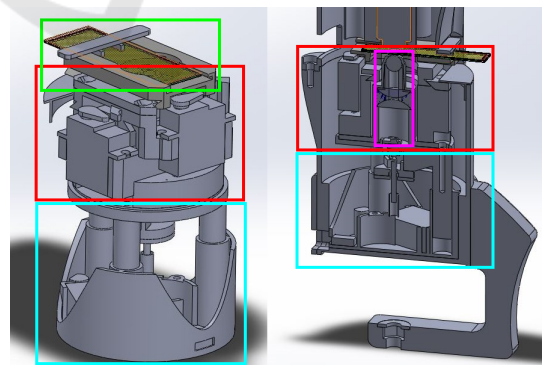


Figure 4: Render model of the motorized automated stage with the identification of the 4 modules: Z-axis (cyan); X/Y axes (red); Illumination (purple); and Smear holder (green).

3.3.2 Electronics

The power board was designed to power the 3 actuators (stepper and two servos) and the illumination LED using only the power from a USB connection with 5V and 500 mA. Almost any modern smartphone has USB-OTG interface that allows the connection of USB peripherals. To be fully compatible with the μ SmartScope, it needs to support, at least, the normal power standard enumerated above. Some manufacturers do not use this standard in their devices and are not supported since these devices are not capable of powering the μ Stage. An image of the developed PCB can be observed in Fig. 5, and the electronic system is composed by:

- **Stepper motor:** The used stepper motor is a 28BYJ-48 5V, which is the cheapest stepper motor found in common electronic stores. This was a major point in choosing the motor since the replication of the μ SmartScope should be easy and cheap in any part of the world. It is controlled by a DRV8836 from Texas Instruments with current limited to 200 mA, and capable of 512 steps per full rotation. Since we are using a standard M3 threaded rod, we have a theoretical resolution of around 1 μ m. Furthermore, a simple push-button switch is placed in the Z axis to provide a way to locate the position when the device is turned on.
- **Two servo motors:** The used servo motors are the Hitec HS-55 5V, which is the cheapest micro servo motor found in common electronic stores. Controlled directly by PWM output and limited to 200 mA, their rotation is directly used to generate the linear movement. The servo head has a size of 13mm meaning that this is our maximum displacement. Using the 90° travel with 2.5° per step, we have 36 steps available while we only need 10 per axis;
- **Illumination:** Since the illumination depends on the sample under analysis, the control board provides an output based on a power Mosfet capable of providing 150mA at 5V. This power can be controlled by changing the PWM duty cycle of the output.
- **Control:** An ATmega32u4 is used to control all the logic of the system, which contains native USB communications and plenty of GPIO ports and PWM support. The native USB connection is seen as a serial port in the smartphone using the *USB serial for Android* library (Wakerly, 2012). Moreover, an API for Android was developed to allow interaction with the stage. This API was made to be as simple as possible to integrate in

any app, providing every function needed to fully control the stage (i.e. stepping in X, Y and Z axes, as well as control the LED light).

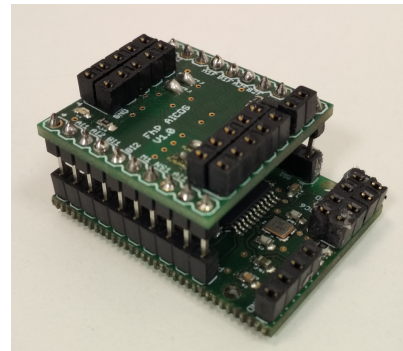


Figure 5: Prototype PCB to control the μ Stage.

4 AUTOMATED FOCUS

The traditional focusing method in microscopy is usually achieved by manually adjusting the vertical position of the smear stage, in order to obtain a focused image of the smear. However, for screening processes that require the analysis of a huge amount of positions per specimen, this process clearly becomes a cumbersome task. As an illustrative example, for the analysis of malaria-infected blood smears, it is recommended the analysis of 100 different positions for a single specimen. Thus, taking advantage of developed motorized automated stage and real time feedback retrieved from the smartphone camera sensor, it became clear that it is fundamental to develop an automated focus approach that ensures autonomous acquisition of focused smear images.

Automated focus is a long standing topic in the literature and several focus algorithms have been proposed (Krotkov, 1988; Shih, 2007), yet the search for the proper algorithm still remains an open topic, since it can highly depend on the resolution of the camera sensor and visual characteristics of the specimen. Generally an autofocus system includes three components: focusing region selection, focus measurement and peak search. In this section it will be presented a description of those components to obtain microscopic images from thin blood smears infected with malaria parasites.

Due to lens constraints, it is not possible to obtain the optical circle with maximal focus in the whole area. Therefore, for each frame given by the camera sensor, this automated focus algorithm considers the central square of the previewed image, with size equal to one third of previewed image (smallest of the

height and weight value) to be the region with maximum focus, as portrayed in Fig.7.

4.1 Focus Metric

Taking into consideration several works on the literature targeting the automatic focus for microscopic devices using image processing, in this work we selected a wide range of focus metrics already proposed that were considered highly relevant for automatic focusing for testing and comparison. In detail, we tested: derivative-based as the Brenner gradient and the Tenenbaum gradient; statistics based, like the normalized variance; histogram-based, as entropy; and intuitive algorithms, like thresholded content (Sun et al., 2005; Liu et al., 2007). After this comparative analysis, the standard deviation (STD) of the Tenenbaum gradient (Tenenbaum, 1970) was considered the most discriminative focus metric to differentiate better a focused point in the focus curve, i.e. in the variation of the metrics while the Motorized Automated Stage is ascending in the vertical axis (see Fig.6). The Tenenbaum gradient is obtained by convolving the previously selected central square of the image with Sobel operators, and by summing the square of gradient vector components:

$$TENG = (G_x(i, j)^2 + G_y(i, j)^2), \quad (2)$$

where G_x and G_y are the horizontal and vertical gradients computed by convolving the focus region image with the Sobel operators. From the previous equation, the STD and the mean values are extracted.

4.2 Focus Logic

The developed automated focus logic has three distinct phases: the Rough, Precise, Ending phase (see Fig.6). The main concept behind the proposed focus logic relies on following concept: the Motorized Automated Stage starts at a bottom position (called the reset position), and while is going up in the Z axis (i.e. the vertical axis), the value of the selected focus metrics starts to increase. The usage of three different phases in the focus logic is directly related with the length of the Z steps. Particularly, a pre-defined length of the Z step is associated to each phase, so while the stage is going up and the metric increases, the focus logic evolves from the Rough phase (Z steps with maximum length) to the Ending phase (Z steps with minimum length).

To better understand the focus logic, please see in Fig.6 where it is presented the behavior of the Tenenbaum metrics while the motorized stage goes up. The first step of the algorithm consists in resetting the

stage to a predefined Z step that is below the focus point (Rough phase). While ascending, in each Z step an image frame is captured and the selected focus metrics are evaluated in order to infer the next move: either stay in the same stage and move up or go to next stage and adapt Z step length. The focus curve for the selected focus metric is usually composed by two local maxima, where the second corresponds to the best focused image region. So a threshold is dynamically defined when the first local maximum is reached, and a focus image is selected and saved only after this threshold is overcome and a new maximum value exists. By doing this, we ensure that the last image saved is the one with best focus quality, while minimizing memory allocation of the algorithm. Moreover and because the stage can suffer some “jumps” leading to metrics behavior different than the one presented, we included a failure index metric which after 3 failures leads the motorized stage to reset.

5 RESULTS

In this section we present the obtained results in terms of Resolution, Field of View and Illumination of the obtained images using the μ SmartScope, as well as an analysis of the μ Stage performance in terms of steps precision/resolution and power consumption.

5.1 Resolution

The magnified images of the smears obtained with the μ SmartScope must have an appropriate resolution over a sufficiently large area, so a conclusive decision about the presence of a specific infectious agent can be made. The 1951 USAF resolution test chart is a resolution test pattern conforming to MIL-STD-150A standard, set by US Air Force in 1951. It is still widely accepted to test the resolving power of optical imaging systems such as microscopes, cameras and image scanners. One example is the READY OPTICS USAF 1951 Microscope Resolution Target, which is a target embedded in a standard microscope slide, suitable for oiled objectives and oiled condensers. In terms of resolution, the target allows to check a minimum spacing between lines of 0.197 nm.

Microscopic images of the READY OPTICS USAF 1951 Microscope Resolution Target with 1000x magnification were acquired the μ SmartScope and with the Bresser Microscope-5102000-Erudit DLX (see Fig. 8). Both systems use similar objectives and eyepieces, so the main goal is to evaluate image resolution of the μ SmartScope.

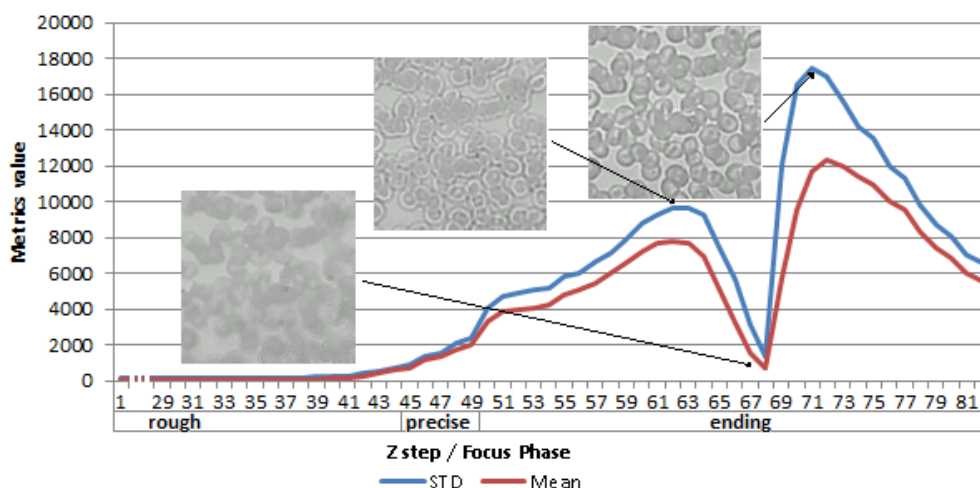


Figure 6: Focus curve of the Tenenbaum metrics for the central square of the image, i.e. variation of the metrics while the Motorized Automated stage is ascending in the vertical axis.

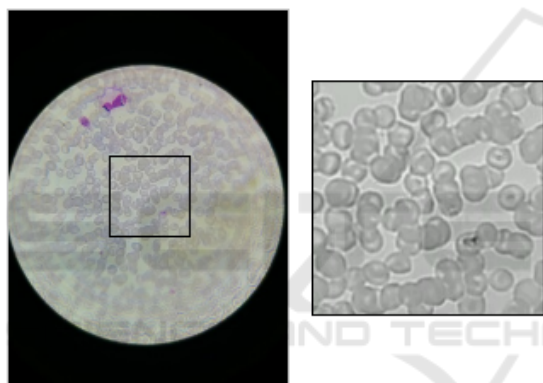


Figure 7: Focused image obtained using the μ SmartScope, and respective central square used by the automated focus algorithm.

To determine the resolution of the μ SmartScope and compare it to the resolution of the Bresser Commercial Microscope, the images acquired with the separate systems were converted to grayscale and the analysis focused on Group 10, which was the smallest resolvable group. In order to determine the smallest resolvable Element of Group 10 in both horizontal and vertical orientations, the images were firstly converted to grayscale and a line for each of the 6 bars of that Element were drawn. Each line starts and ends in a background pixel, and intersects perpendicularly the respective bar. All pixel values of each line were used to calculate the Michelson contrast, which was assigned to the respective bar. In each direction of each Element, the bar with minimum Michelson contrast was selected for analysis purposes (see Fig. 9).

It was defined that an Element is considered resolvable on a particular direction if the minimum

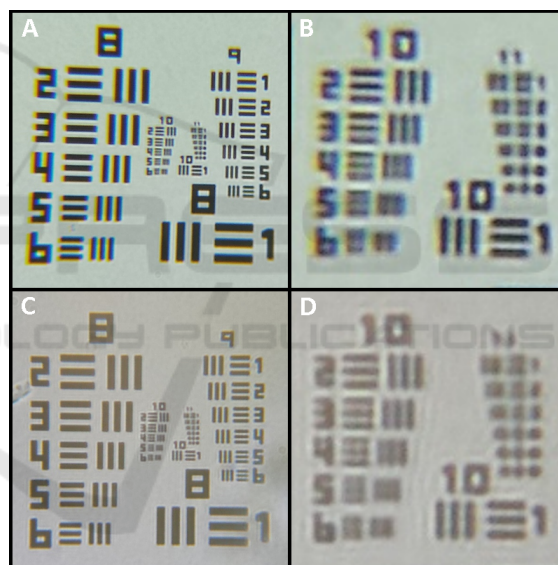


Figure 8: Images of READY OPTICS USAF 1951 microscope resolution target: A) acquired using the μ SmartScope; B) Detail of Group 10 using the μ SmartScope; C) acquired using Bresser Microscope - 5102000 - Erudit DLX 20x-1000x; D) Detail of Group 10 using the Microscope.

Michelson contrast was 0.1. Thus, Element 3 was defined as the minimum resolvable Element for the μ SmartScope, which gives a minimum resolution of $0.388\mu\text{m}$ on both directions. For the Bresser Commercial Microscope, Element 4 was selected as the minimum, which corresponds to a resolution of $0.345\mu\text{m}$ for both directions. Although the μ SmartScope present a slightly lower resolution, it is clear on Fig. 9 that both directions have a more homogenous behavior.

ior in terms of resolution, while in the Bresser Microscope there is an evident discrepancy between the resolving power on different directions. The lower values of Michelson contrast for the μ SmartScope might be caused by the limitation in terms of the maximum power rate of the smartphone, since both the illumination and motorized automated stage must be powered by USB-OTG. Thus the power that feeds the LED is limited, which diminishes the intensity of the LED and consequently the image contrast.

5.2 Field of View

Resolution and field of view are inversely linked in standard laboratory microscopes. In order to obtain microscopic fields with both high magnification and resolution, the usage of objectives with higher numerical aperture is required, which results in smaller Field of Views (FOV) (Pirstill and Cot, 2015). To determine the FOV of the μ SmartScope, images of the READY OPTICS USAF 1951 Microscope Resolution Target were acquired and used to estimate the pixel-microns relationship. The exact distances between bars of a specific Element is given by the specifications of the resolution target, particularly Element 2 and 3 of Group 8 corresponds to $1.740\mu\text{m}$ and $1.550\mu\text{m}$, respectively. By measuring the number of pixels between bars of this 2 Elements on the acquired image, a relationship of $0.085\mu\text{m}/\text{pixel}$ was obtained for Element 2 and $0.084\mu\text{m}/\text{pixel}$ for Element 3. So we considered the average value, i.e. a relationship of $0.0845\mu\text{m}/\text{pixel}$. Furthermore, the number of pixels for the vertical and horizontal axis that passes through the center of the visible optical circle of the acquired image were determined. These values were then combined with the previously calculated $\mu\text{m}/\text{pixel}$ relationship, in order to estimate the FOV of the visible optical circle, with $214.38\mu\text{m}$ and $206.87\mu\text{m}$ for the vertical and horizontal axis, respectively.

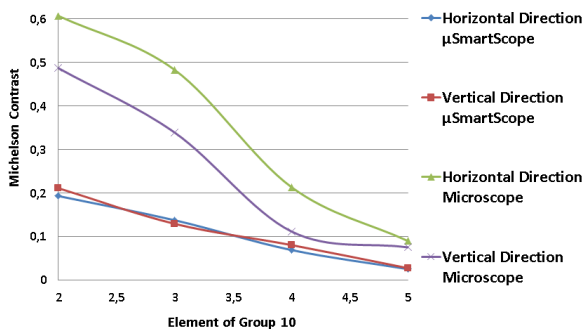


Figure 9: Minimum Michelson contrast for USAF Resolution Target Elements of Group 10.

5.3 Illumination

In order to evaluate the uniformity of the illumination of the LED coupled to the proposed condenser, an image was acquired with a blank microscope slide (see Fig. 10.A). A diagonal line scan was considered to evaluate the variation of pixels intensity along this line. A total of 200 pixel boxes were considered, equally spaced and with size 10×10 . For each of those boxes the mean and standard deviation were collected (see Fig 10.B and 10.C). Despite small pixel intensity variations probably caused by dust or components floating in the immersion oil, this results demonstrate that we can achieve a substantially uniform illumination with low noise with the proposed set up.

5.4 μ Stage

The μ Stage was analyzed in terms of precision and resolution of the X/Y and Z steps, as well as in terms of power consumption.

5.4.1 Precision and Resolution

While testing the usage of the μ Stage, we found out that the precision of each axis is affected by the fact that all moving parts are 3D printed. Since plastic imperfections and particles can be present in the sliding portions of the parts, this leads to different displacements in each step. In Fig. 11 is presented the results for the displacement of the X, Y and Z axis, where 100 steps were taken and each one measured using a digital caliper (Mitutoyo Absolute) with resolution of $0.01\text{mm} \pm 0.02\text{mm}$. Each measure was grouped per value and the frequency plotted.

For the X and Y steps, a clear variation of the step size is depict in Fig 10.A. This behavior is mainly caused by the non-linear movement of the servo (previously described in section 3.3.1), as well as by the

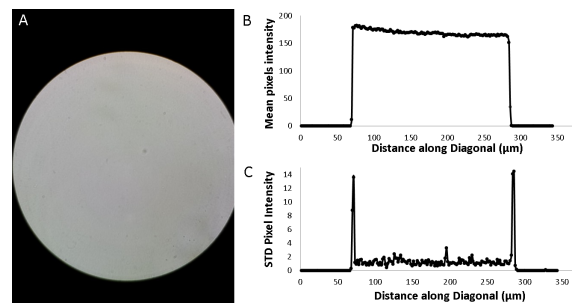


Figure 10: Illumination uniformity analysis for Prototype: a) Original image; b) Mean pixel intensity of the 10×10 pixel boxes on the diagonal direction; c) Standard deviation of the 10×10 pixel boxes on the diagonal direction.

imperfections of the printed parts. Nevertheless, we obtained an average displacement of $330\mu\text{m}$ with a standard deviation of $81\mu\text{m}$, which proved to be a suitable approach for our solution. Taking into account that the main goal of the X and Y steps is to displace the smear into a different position and acquire an image of a new microscopic field, the average displacement provided by this approach is marginally higher than the FOV determined in section 5.2, which consequently means that we are obtaining a new microscopic field every time we take a X or Y step.

Regarding the Z axis, our caliper is not able to measure such small steps. To estimate the average step size, one full revolution of the motor was considered (which corresponds to 512 steps), and the respective displacement was measured 100 times. This distance was then divided by the number of steps, in order to estimate the travel of a single step. As we can see in Fig 10.B, the steps are less dispersed, but a significant variability is still verified. Each step corresponds to an average of $0.98\mu\text{m}$ with a standard deviation of $0.18\mu\text{m}$, which gives an indication that our steps in the Z axis are within the theoretical values.

Although we have a small step-size in the Z axis, we observed that the movement is not smooth and the variability in the step size leads to some “jumps” while focusing the microscopic field. At 1000x magnification this can have a significant impact in obtaining the ideal focus point of the smear. It worth noting that this is the reason why we can not simply move

Table 1: Power consumption test results.

Smartphone	Average Current (mA)	Average Power Consumption (W)	Autonomy (min)
Samsung S5	208.64	1.043	164
Nexus 5	201.34	1.006	149

the Z axis to a specific pre-defined position that corresponds to the focus point, in order to focus the specimen. Thus, the automatic focus methodology proposed on section 4 plays a critical role in the compensation of this irregular behavior, and consequently in the acquisition of focused images autonomously.

It worth noting that the overall image acquisition process involves: autonomous control of the Z axis for autofocusing, capture the image in the focus point, and autonomous control of the X/Y axes to the next microscopic field (where this process restarts if we want to acquire a new image). We tested the autonomous acquisition of 100 images using a LG Nexus 5, which took in average 80 seconds per image, and 94 of the images were considered focused.

5.4.2 Power Consumption

In order to ensure that we never go over the maximum power rate of the smartphone, the whole system power consumption is always under 400mA at 5V. This is achieved by allowing only one actuator moving at any given time. In Table 1, the power consumption of the system can be observed together with the autonomy for the tested smartphones. The profile tested was as close as possible to the real one, i.e. the smartphone was acquiring views continuously with the screen off and in flight mode until it shut down due to low battery.

It worth noting that we are currently using the smartphone battery to simultaneously powering the actuators of the μStage , the LED light, acquired data continuously with the optic sensor and process each acquired frame for the automatic focus of the smear. Considering the current battery capacity of smartphones, this obviously represents a huge burden in terms of power consumption, and it is clear that the current autonomy of the system is low for a day of continuous use. As an alternative, one can consider the usage of at least two smartphones to allow the acquisition of images 24h per day, or the usage of a power bank coupled to a OTG splitter cable, which we are considering to include in the next version of the $\mu\text{SmartScope}$ system.

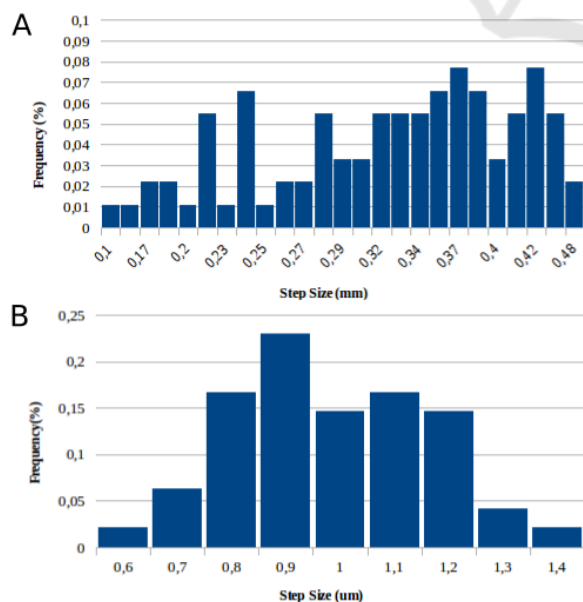


Figure 11: Frequency of measured step size values after 100 repetitions. A) X and Y axes; B) Z axis.

5.5 Applicability Examples

The μ SmartScope was used to acquire microscopic images of reference blood smears with different parasites, which are responsible for the most relevant neglected tropical diseases that can be detected through microscopic examination (see Fig 12). Particularly, the following smears were used: thick blood smear infected with malaria parasites (*P.falciparum* species); thin blood smear infected with malaria parasites (*P.ovale* and *P.malariae* species); thin blood smear infected with Chagas parasites (*Trypanosome cruzi* species); and thick blood smear infected with Lymphatic Filariasis parasites (*Brugia malayi* and *Wuchereria bancrofti* species).

Furthermore, to highlight the versatility of the developed system, a liquid-based Pap smear with high grade squamous lesions was also tested, which is associated with precancerous changes and high risk of cervical cancer. For the analysis of this smear, a magnification of 400x is required, so we had to adapt the optical set up of the μ SmartScope, which consisted in the simple procedure of changing the Bresser Planachromat 100x oil-immersion objective for the Bresser Planachromat 40x (Bresser #5941540).

To finalize, considering the acquired images and the feedback received by the specialists that helped us collect the smears, we can state that very promising results were obtained. For all the tested smears, the detection of the considered blood parasites and the precancerous cells on the cervix was considered possible through images acquired via the μ SmartScope.

6 CONCLUSIONS

In this paper, we present a 3D-printed microscope that can easily be attached to a wide range of mobile device models. This is the first proposed smartphone-based alternative to conventional microscopy that allows autonomous acquisition of a pre-defined number of images at 1000x magnification with suitable resolution, by using a motorized automated stage fully powered and controlled by a smartphone, without the need of manual focus of the smear.

All the components of the proposed device are described and properly evaluated. In terms of the Optical Module, a minimum resolution of $0.388\mu\text{m}$ was determined, with a FOV of $214.38\mu\text{m}$ and $206.87\mu\text{m}$ for the vertical and horizontal axis that passes through the center of the visible optical circle, respectively. Regarding the Illumination Module, the LED light coupled to the proposed condenser demonstrated to achieve an uniform illumination suitable for bright-

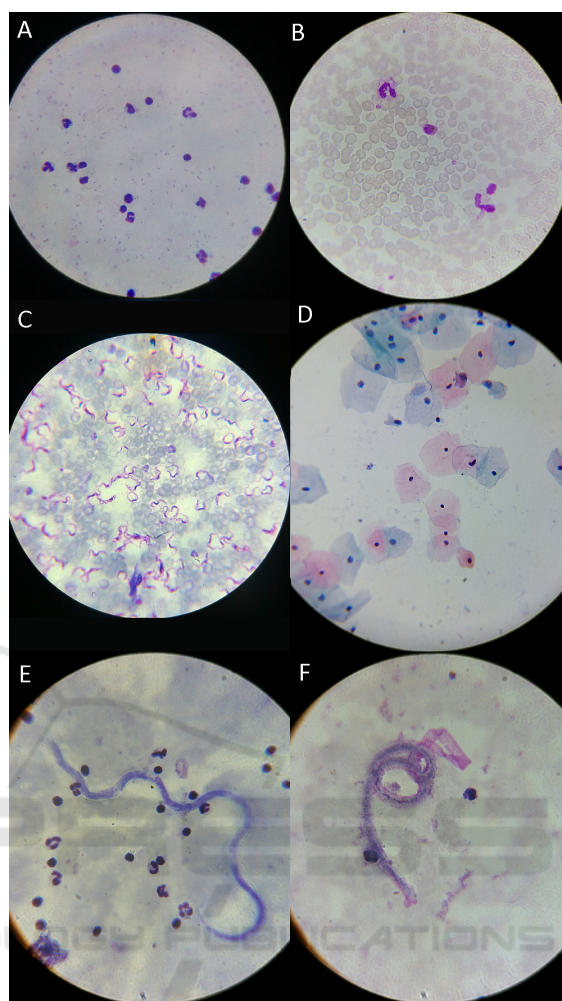


Figure 12: Images of different smears acquired with the μ SmartScope: a) Thick blood smear infected with malaria parasites (*P.falciparum* species); b) Thin blood smear infected with malaria parasites (*P.ovale* and *P.malariae* species); c) Thin blood smear infected with Chagas parasites (*Trypanosome cruzi* species); d) Liquid-based Pap smear with high grade squamous lesions; e) Thick blood smear infected with Lymphatic Filariasis parasites (*Brugia malayi* species); f) Thick blood smear infected with Lymphatic Filariasis parasites (*Wuchereria bancrofti* species). Images a), b) and c) were acquired with a LG Nexus 5, while images d), e) and f) with a Samsung Galaxy S5. All images were acquired with magnification of 1000x, except image d) which has magnification of 400x.

field microscopy. In terms of the Motorized Automated Stage (μ Stage), we achieved an average resolution of $330\mu\text{m}$ (with a standard deviation of $81\mu\text{m}$) for the X and Y steps and an average resolution of $0.98\mu\text{m}$ (with a standard deviation of $0.18\mu\text{m}$) for the Z steps.

Several smears infected by different blood parasites responsible for the most relevant neglected tropi-

cal diseases were used to test the device. The acquired images showed that it was possible to detect those agents through images acquired via the μ SmartScope, which clearly illustrate the huge potential that this device can have, specially in developing countries with limited access to healthcare services.

As future work, we want to tackle several of the detected issues in order to achieve a more robust version of the μ SmartScope system. In particular, we want to solve the significant negative impact of occasional plastic imperfections (originated by the 3D printing process) in the precision of the μ Stage, as well as the currently low autonomy of the system for continuous usage.

ACKNOWLEDGEMENTS

We would like to acknowledge the financial support from North Portugal Regional Operational Programme (NORTE 2020), Portugal 2020 and the European Regional Development Fund (ERDF) from European Union through the project 'Deus ex Machina: Symbiotic Technology for Societal Efficiency Gains', NORTE-01-0145-FEDER-000026.

REFERENCES

- Arpa, A., Wetzstein, G., Lanman, D., and Raskar, R. (2012). Single lens off-chip cellphone microscopy. pages 23–28. IEEE.
- Cybulski, J. S., Clements, J., and Prakash, M. (2014). Foldscope: Origami-Based Paper Microscope. *PLoS ONE*, 9(6):e98781.
- Dolgin, E. (2015). Portable pathology for Africa. *IEEE Spectrum*, 52(1):37–39.
- Krotkov, E. (1988). Focusing. *International Journal of Computer Vision*, 1(3):223–237.
- Liu, X., Wang, W., and Sun, Y. (2007). Dynamic evaluation of autofocus for automated microscopic analysis of blood smear and pap smear. *Journal of microscopy*, 227(1):15–23.
- Pirnstill, C. W. and Cot, G. L. (2015). Malaria Diagnosis Using a Mobile Phone Polarized Microscope. *Scientific Reports*, 5:13368.
- Quinn, J., Andama, A., Munabi, I., and Kiwanuka, F. (2014). Automated Blood Smear Analysis for Mobile Malaria Diagnosis. In *Mobile Point-of-Care Monitors and Diagnostic Device Design*, Devices, Circuits, and Systems.
- Rosado, L., Costa, J. M. C. d., Elias, D., and Cardoso, J. S. (2016). A Review of Automatic Malaria Parasites Detection and Segmentation in Microscopic Images. <http://www.eurekaselect.com>, 14(1):11–22.
- Shih, L. (2007). Autofocus survey: a comparison of algorithms. In *Electronic Imaging 2007*, pages 65020B–65020B. International Society for Optics and Photonics.
- Smith, Z. J., Chu, K., Espenson, A. R., Rahimzadeh, M., Gryshuk, A., Molinaro, M., Dwyre, D. M., Lane, S., Matthews, D., and Wachsmann-Hogiu, S. (2011). Cell-Phone-Based Platform for Biomedical Device Development and Education Applications. *PLoS ONE*, 6(3):e17150.
- Sun, Y., Duthaler, S., and Nelson, B. J. (2005). Autofocusing algorithm selection in computer microscopy. In *2005 IEEE/RSJ International Conference on Intelligent Robots and Systems*, pages 70–76. IEEE.
- Switz, N. A., D'Ambrosio, M. V., and Fletcher, D. A. (2014). Low-Cost Mobile Phone Microscopy with a Reversed Mobile Phone Camera Lens. *PLoS ONE*, 9(5):e95330.
- Tenenbaum, J. M. (1970). Accommodation in computer vision. phd dissertation. Technical report, DTIC Document.
- Tseng, D., Mudanyali, O., Oztoprak, C., Isikman, S. O., Sencan, I., Yaglidere, O., and Ozcan, A. (2010). Lens-free microscopy on a cellphone. *Lab on a Chip*, 10(14):1787–1792.
- Uttinger, J., Becker, S. L., Knopp, S., Blum, J., Neumayr, A. L., Keiser, J., and Hatz, C. F. (2012). Neglected tropical diseases: diagnosis, clinical management, treatment and control. *Swiss Medical Weekly*, 142:w13727.
- Wakerly, M. (2012). Usb serial for android.
- WHO, W. H. O. (1991). *Basic malaria microscopy*.
- Zachary, G. (2015). Technology alone won't improve health in Africa [Spectral lines]. *IEEE Spectrum*, 52(1):7–7.